Archaeomagnetic dating and magnetic characterization of ceramics from the Paquimé, Casas Grandes region, Chihuahua, Mexico

Luis Manuel Alva-Valdivia, Alejandro Rodríguez-Trejo, Rafael Cruz-Antillón, Gwenaël Hervé, Mireille M. Perrin, M. M. Salgado-Saito, Ahmed Nasser Mahgoub

Archaeomagnetic dating and magnetic characterization of ceramics from the Paquimé, Casas Grandes region, Chihuahua, Mexico

Alva-Valdivia, L. M. [1], Rodríguez-Trejo A. [2], Cruz-Antillón, R. [3], Hervé, G. [4], Perrin, M. [5], Salgado-Saito, M. M. [6] and Mahgoub A. N.[1, 7]

[1] Universidad Nacional Autónoma de México: Instituto de Geofísica, Laboratorio de Paleomagnetismo, Ciudad Universitaria 04510, Ciudad de México, Mexico.

[2] Centro de Geociencias, Universidad Nacional Autónoma de México, Blvd. Juriquilla 3001, Querétaro 76230, México.

[3] Instituto Nacional de Antropología e Historia, Sede Chihuahua, Mexico.

[4] Laboratoire des Sciences du Climat et de l'Environnement/IPSL, CEA, CNRS, UVSQ, Université Paris-Saclay, Gif-sur-Yvette, France

[5] Aix Marseille Univ, CNRS, IRD, INRA, Coll France, CEREGE, Aix-en-Provence, France.

[6] Universidad Nacional Autónoma de México: Facultad de Ciencias, Ciudad Universitaria 04510, Ciudad de México, Mexico.

[7] Geology Department, Assiut University, Assiut, 71516, Egypt

Corresponding author: lalva@igeofisica.unam.mx

Abstract

Casas Grandes is a prehistoric culture area located between Chihuahua, northern Mexico, and New Mexico, southwest of United States of America. It had an intense occupation with large buildings during the ceramic period, from 0 to 1450 AD, developing very particular painted potteries. In this study, magnetic properties and archaeointensity experiments were investigated on two special ceramic types called Mimbres and polychrome Ramos. They come from four archaeological sites from Casas Grandes region in northern Chihuahua:

Paquimé, Villa Ahumada, Galeana, and Samalayuca. Archaeological timing and typology assign Mimbres and Ramos to an age period between 900–1450 AD, but no absolute ages are available. Magnetic properties show that Mimbres and Ramos have different magnetomineralogical properties, suggesting that pottery making materials were different. Mean archaeointensity results were obtained from nine different pottery sherds, five from Mimbres and four from Ramos polychrome, for a total of 35 specimens. Intensity value range from 49-59μT for Mimbres type and from 41-49 μT for Ramos type. Archaeomagnetic dating was performed using the SHAWQ2k global model and the Maghoub regional paleosecular variation curve. Archaeomagnetic dating give an absolute age range of 960-1100 AD for Mimbres type, and of 1300–1600 AD for Ramos samples, confirming that both ceramic types were manufactured at different times. These results highlight the potential of archaeomagnetism to precise the chronological framework of Casas Grandes culture.

Keywords: archaeomagnetism, ceramics, Paquimé, Casas Grandes, archaeomagnetic dating, Mexico

1. Introduction

Archaeomagnetism is the magnetic study of different archaeological records, mainly baked clays (e.g. kilns, hearths, ceramics). These baked materials contain ferromagnetic particles (ca. 0.1% concentration) that acquire thermal remanent magnetization (TRM), parallel to the direction (declination and inclination) of the ambient Earth's magnetic field (EMF) and proportional to its intensity at the time of the last cooling. This TRM and hence the EMF ancient direction (archaeodirection) and intensity (archaeointensity) remain preserved unless another firing event occurred, or it was disturbed by lightning or chemical alterations for example. In contrast to the ease of obtaining archaeodirection with a certain degree of reliability, the archaeointensity estimation is still more difficult because the ferromagnetic particles can have non-ideal magnetic properties as low thermal stability or large (> 1 μm) multi-domain grain size. These non-ideal behaviours violate the fundamental conditions needed to apply the most widely used archaeointensity method (Thellier & Thellier, 1959) and its derivatives (Coe, 1967; Aitken et al., 1988; Tauxe and Staudigel, 2004).

The EMF is continuously changing in time, a phenomenon called palaeosecular variation (PSV). If TRM data obtained from well-dated archaeological or igneous material have a suitable spatio-temporal distribution, then the PSV can be described for any geographic location by global spherical harmonic models, such as: ARCH10k.1 (Constable et al, 2016), ARCH3k.1 (Korte et al., 2009), CALS10k.1b (Korte et al., 2011), CALS10k.2 (Constable et al., 2016), SHA.DIF.14k (Pavón-Carrasco et al., 2014), COV-ARCH and COV-LAKE (Hellio and Gillet, 2018), BIGMUDI4k.1 (Arneitz et al., 2019), and SHAWQ2K (Campuzano et al., 2019). Also, regional PSV reference curves can be generated for a given area, using full-vector (direction and intensity) (e.g. Kovacheva et al., 2014; Tema and Lanos, 2020), directional (e.g. Hagstrum and Champion, 2002), or intensity (e.g. De Marco et al., 2008; Hervé et al., 2017) data. For Central Mexico, three regional curves of the geomagnetic field intensity were recently generated (Goguitchaichvili et al., 2018a; Hervé et al., 2019; Mahgoub et al., 2019a). The curves of Goguitchaichvili et al. (2018) and Mahgoub et al. (2019a) were built using a bootstrap approach (Thébault and Gallet, 2010), but both curves have different input and data selection strategies. Goguitchaichvili et al. (2018) curve was constructed for the past 3000 years using intensity data previously published from Mexico and Southern USA. An update of this curve has been recently released (García et al., 2020). We note that some of the input data in these curves were corrected with a contested anisotropy method (for details see Hervé et al., 2019). Mahgoub et al. (2019a) full-vector curve covers the past 46 ka and was constructed from their data (Mahgoub et al., 2019b) as well as from previous data published from Central Mexico, which were selected after application of strict selection criteria and reassessment of previous ages. The intensity curve of Hervé et al. (2019) was determined using a Bayesian method (Hervé and Lanos, 2018), with selection criteria similar to those of Mahgoub et al. (2019a), but without the high-quality intensity data of Mahgoub et al. (2019b). For northern Mexico, a PSV master curve has yet to be constructed, although previous palaeomagnetic (e.g. Alva-Valdivia et al., 2019; Rodríguez-Trejo et al., 2019b) and archaeological (Pails, 2017; Mathiowetz, 2019) studies showed the wealth of this region with volcanic and archaeological materials.

The greatest benefit of PSV reference curves is that they can be used in archaeomagnetic dating (Aitken, 1966; Eighmy and Sternberg, 1990; Sternberg, 2008). Archaeomagnetic dating consists in the comparison of the direction and/or intensity of undated material with a

PSV reference curve (regional or global). This dating technique was successfully applied in different regions over the globe, such as northwestern America (Hagstrum & Blinman 2010) and Europe (e.g. Arrighi *et al*., 2006; Schnepp and Brüggler, 2016; Tema *et al*., 2019), accordingly it can be used as an alternative to other traditional methods (e.g. radiocarbon and thermoluminescence dating). In Mexico, previous studies have confirmed the validity of this method with Holocene erupted lavas (e.g. Böhnel et al., 2016; Mahgoub et al., 2017, 2018) and also archaeological artefacts (e.g. Goguitchaichvili et al., 2016; 2017), located in Central Mexico. So far, no archaeomagnetic dating has been applied to the region of northern Mexico.

In this study, magnetic properties and archaeointensity data are presented for two types of potteries (Ramos and Mimbres) collected from four archaeological sites belonging to the culture of Casas Grandes, Chihuahua, northern Mexico. These potteries were previously catalogued by archaeologists as being of the Mimbres (designs black or red on white fund) and Ramos (polychrome) types, with a global age period ranging from 900 to 1450 AD (Dean & Ravesloot, 1993; Kelley & Phillips Jr., 2017; Ravesloot *et al*., 1995; Stewart *et al*., 2005; Whelan & Minnis, 2009). The main objective of this study is to test the potential of archaeomagnetic dating at this period in Northern Mexico.

2. Archaeological setting

The archaeological materials of this study are from the Casas Grandes and Mimbres cultures, located at the northwest of Chihuahua (Mexico) and southwest of New Mexico (US), respectively (Fig. 1). Both belong to the major culture called 'Mogollon' that, together with 'Pueblo Ancestral' (before Anasazi) and 'Hokoham', constitutes the cultural macro-region 'Oasisamerica' or 'Aridoamerica' (Kirchhoff, 1954).

Since many years, the Casas Grandes culture, and its capital Paquimé, has caught the attention of specialists (Bandelier 1890; Brand 1943; Di Peso 1974; Kelley & Phillips Jr., 2017; Lumholtz 1904; Sayles 1936; Whalen & Minnis, 2001, 2009). Chronological framework of Casas Grandes culture was recently revised by Pailes (2017). Between 1959 and 1961, Charles Di Peso (Di Peso *et al*., 1974) started a very intensive and rigorous archaeological study in Paquimé, recovering large amount of potteries, shells, and organic

materials that allowed the first chronology of the region. He identified two important cultural branches: pre-ceramic and ceramic.

2.1 Pre-ceramic Period

This is a large period that starts ca. 12,500 BC, when the inhabitants were 'hunters-gatherers' in the Paleocene. This period is called 'Paleoindio' characterized mainly by the Folsom and Clovis grooved arrows found in Chihuahua (Di Peso, 1965). After the Paleoindian period, started the 'Archaic' period (9000 BC to 0), characterized by semi-nomadic life-style and the appearance at the end of an early agriculture.

2.2 Ceramic Period

This period is divided in four main phases:

1) The Plainware period (1 to 700 AD) corresponds to the first ceramic traditions, with brown to red color pots, jars, and pipes without decoration.
2) The Viejo Period (700 to 1200 AD) corresponds to the establishment of Paquimé city with related settlements in surrounding caves. This period is divided in two phases: Early Viejo and Late Viejo (Dean & Ravesloot, 1993; Kelley & Phillips Jr., 2017; Ravesloot et al., 1995; Stewart et al., 2005; Whalen & Minnis, 2009). At the end of this period appear evidences of exchange with other cultures from Central and northern Mexico as well as southwest of United States, with many shells, turquoise counts and cooper artifacts.
3) The Medio Period (1200 to 1450 AD) corresponds to the full development of the Casas Grandes culture. Paquimé has grown with a strong increase of the population, the development of economy, politics, social and culture, and the maximum architectural magnificence. One of the most conspicuous features of this period in the Casas Grandes region is a remarkable polychrome ceramic, with thinner textures, and a variety of sophisticated designs with anthropomorphic and zoomorphic shapes.
4) The Late Period corresponds to the start of the waning of Paquimé (Di Peso, 1974).

2.3 Sampled potteries

24 sherds were collected by R. Cruz-Antillón at the surface of different sites in the Casas Grandes region: Paquimé, Galeana, Villa Ahumada and Samalayuca (Fig. 1, Table 1). This work was intended as a pilot study to test the efficiency of archaeomagnetic dating for this

ceramic type. If the results are positive, the archaeomagnetic dating technique could be applied to other sherds of this region for which the stratigraphy between archeological layers is not well defined and no other dating is possible.

The sherds were classified accordingly to their typology (Mimbres and Ramos polychrome), characterized by designs unique in the region (Fig. 2). The Mimbres ceramic belongs to the period 1000 to 1150 AD and is distinguished by its white color and motifs painted in black, generally jars. The Ramos polychrome ceramic is characterized by matte cream-orange decors with red and black color, and very eccentric shapes. This ceramic is typical of the Paquimé Medio period between 1200 to 1450 AD.

3. Laboratory procedures

We first performed thermomagnetic experiments with the recording of susceptibility (k) as a function of temperature, the so-called k-T curves. Representative samples were heated in air up to 600-700ºC with a MFK-FA susceptibility-meter (Agico, Kappabridge) and then cooled back to room temperature. Curie temperature (Tc) value(s) and the type of the ferromagnetic minerals were investigated from these curves, as well as the thermal stability of the samples. We measured the hysteresis properties and the isothermal remanent magnetization (IRM) spectra, by using a Princeton AGFM Micromag 2900 apparatus, in fields up to 1.2 Tesla at room temperature. From them, saturation magnetization (M_s), saturation remanent magnetization (M_{rs}), coercive force (H_c) and remanent coercive force (H_{cr}), were determined. The ratios of these parameters provide rough information on the size distribution of the magnetic domains and the different mixtures of magnetic minerals contained in the samples (e.g., Day et al., 1977; Dunlop, 2002).

One specimen per sherd, cut on parallelepipedic shape of *ca.* 18×5×3 mm, was thermally demagnetized (ThD) to investigate the number of remanent magnetization components and to define the unblocking temperature ranges. Three to six specimens of each sherd were used for archaeointensity experiments using the Thellier & Thellier (1959) classical double heating method. The Thellier & Thellier (1959) method involves heating a specimen twice with a laboratory-induced magnetic field applied along its two long axes (+ z, -z). Heating was done from 150 to 580 ºC with 10 to 12 steps, and the laboratory field was set to 40 μT.

During the experiments, partial thermal remanent magnetization (pTRM) checks (Coe, 1967) were performed every two temperature steps to check for magneto-mineralogical alteration. The stepwise heating-cooling process was performed using a MMTD24 oven, and the remanent magnetization was measured with a JR6 spinner magnetometer. Results were processed with the ThellierTool 4.22 software (Leonhardt et al., 2004). In order to accept archaeointensity results, the following quality criteria were considered: 1) Number of steps (N) used to calculate the best-fit linear segment on Arai plot (Nagata et al., 1965) higher or equal to 5; 2) Ratio (β) of the standard error of the slope of the best-fit line to the absolute value of the slope lower than 0.15; 3) NRM fraction (f) greater than 30%; 4) Gap factor (g), that reflects closeness of points along Arai plot segment selected for intensity determination (Coe et al., 1978) higher than 0.5; 5) Quality factor ($q=fg/\beta$) higher than 3; 6) Anchored maximum angular deviation (MAD_{anc}; Kirschvink, 1980) lower than 15°; 7) Angular difference (α) between the anchored and the non-anchored best-fit directions lower than 15°; 8) Relative check error (dCK), defined as the maximum difference produced by a pTRM check normalized to the TRM, lower than 10%; and 9) Cumulative pTRM check (dpal; Valet et al., 1996) lower than 15%. In order to calculate a mean archaeointensity at the sherd level, at least 3 specimens must be accepted, and the standard deviation (σ) should not exceed 6 μT. The current selection criteria are similar to sets proposed in other studies, e.g. SELCRIT2 (Biggin et al., 2007) or ThellierTool B (TTB) (Leonhardt et al., 2004).

Ceramics manufacturing process commonly results in preferential alignments of the magnetic grains inducing a TRM anisotropy effect, and this anisotropy has been shown to bias the archaeointensity estimates (Rogers et al., 1979; Aitken et al., 1981). Therefore, it is necessary to correct for this effect by calculating the anisotropy tensor of TRM (Veitch et al., 1984; Chauvin et al., 2000) with six successive heating at 540°C along 6 positions (+x, −x, +y, −y, +z and −z specimen axes), followed by a stability check. The influence of cooling rate on TRM intensity was tested with the procedure described in Chauvin et al. (2000). The duration of the slow cooling was fixed to 5 hours due to experimental constraints, in comparison with the rapid cooling that took *ca.* 45 min. It is worth pointing out that this duration is close to the one provided by experimental archaeology of ceramic production in the American Southwest (Jones-Cervantes et al., 2020).

4. Results

4.1 Magnetic properties

The heating-cooling branches of the k-T curves are shown in Figure 3. According to the Tc values and the degree of reversibility between the heating and cooling curves, samples could be classified into three groups. The first group, which include all sherds of Ramos type, has a single high Tc ranging between 500–580 °C (Fig. 3, PR-2, GR-4, and VAR6), corresponding to a typical behaviour of Ti-poor titanomagnetite (TMag) and/or magnetite (Mag). This group shows a good degree of reversibility indicating thermal stability at high temperatures. The second group of samples is also characterized by a single high Tc ranging from 500–540°C (Fig. 3, CH-3-3, and PM-2) but irreversible curves with the cooling curve rising above the heating curve. The interpreted magnetic mineralogy content of this group is mostly Ti-poor TMag, which transforms after heating to 700 °C in TMag with less Ti and a higher magnetic content. The third behaviour, seen solely in sample PM-1 (Fig. 3), shows two Tc points: the first is ~340 °C while the second Tc ranges from 480 to 560 °C, suggesting coexistence of Ti-poor and Ti-rich TMag (the last one probably created during the experiment). This group is characterized by low degree of reversibility with a large increase of the susceptibility after heating to 700 °C. Samples of this group were not used for archaeointensity experiments. It must be noted that all investigated samples of Ramos belong to the 1st group while the 2nd and 3rd group samples are from Mimbres pottery types.

The hysteresis curves (Fig. 4) present two different shapes indicating diverse mixtures of magnetic mineralogy. The *'potbellied'* shape, observed in 65% of the samples (e.g. Fig. 4: CH-3-1-4, CH3-3-2, VAR-10 and GR-4), shows a typical pseudo single-domain (PSD) behaviour with smaller magnetic grain size (see Fig. 5, Tauxe, et al., 1996, 2002). Other specimens (e.g. Fig. 4: PM-1 and PR-2) present 'wasp-waisted' hysteresis curves, highlighting a mixture of low and high coercivity magnetic minerals, such as titanomagnetite and minor amount of titanohematite. This mixture shows a trend of superparamagnetic (SP) (Tauxe et al. 2002) and larger PSD-like to multidomain (MD) grains. Both shapes can be observed in Mimbres and Ramos polychrome. The larger differences between hysteresis curves before and after the paramagnetic correction shows that the contribution of paramagnetic minerals is higher for specimens PR-2 and CH-3-3-2. Inset in each graph of

241 Figure 4 are the IRM and backfield curves, where the contribution of magnetic components
242 and possible composition can be identified from the saturation magnetization and coercivity
243 values. All samples are dominated by a magnetic component with coercivities below 200-
244 300 mT that corresponds to the Ti-poor titanomagnetite seen in the k-T curves. A high
245 coercivity component, likely titanohematite, is also present in variable proportion. In
246 agreement with hysteresis results, the highest proportion is observed in PM-1 and PR-2
247 samples.

248 Result of hysteresis parameters and ratios are listed in Table 2 and plotted on a Day plot (Day
249 et al., 1977) in Figure 5. This diagram is commonly used to identify the size of the
250 ferromagnetic particles (single-domain SD, pseudo-single domain PSD, multidomain MD,
251 and superparamagnetic SP particles), when the magnetic carriers are only magnetite grains.
252 Here, the presence of a high-coercivity component shifts the specimens, especially PM-1 and
253 PR-2, to the right of the Dunlop (2002) curves. If this prevents to accurately determinate the
254 particle sizes, the Day plot remains relevant to discriminate between the different pottery
255 types, Ramos polychrome being slightly lower than Mimbres samples in the PSD zone.

256 **4.2 Archaeointensity**

257 Archaeointensity experiments were performed on 16/24 pottery sherds, eight from Mimbres
258 and eight from Ramos polychrome ceramic types. These sherds were selected because they
259 exhibit a single component of thermoremanent magnetization and reversible k-T curves.
260 The thirty-six specimens (10 out of 16 sherds) that fulfil the acceptance criteria are listed in
261 Table 3, and representative Arai plots are shown in Figure 6. Archaeointensity statistical
262 parameters indicate that the obtained results are of good quality (Table 3).
263 The TRM anisotropy (ATRM) correction was applied to all accepted archaeointensities and
264 resulted in a decrease of the values by *ca.* 1% to 4%. The cooling rate (CR) effect was tested
265 on eight specimens from PM-2 and PR-1 samples. As correction factors were pretty small
266 and very similar (between 3.4 and 4.9%), an average value of 4% was applied to all accepted
267 anisotropy-corrected archaeointensities. Table 3 lists raw, corrected for ATRM and for CR
268 effects estimates (F_{raw}, F_{ATRM} and $F_{ATRM+CR}$, respectively).

269 Mean archeointensity estimates could be calculated for nine sherds that have at least three
270 accepted specimens. The application of ATRM and CR corrections generally decrease the

standard deviation (Table 3), and the archaeointensity ranges for the Mimbres and Ramos ceramic types are between 49–59 μT and 41–49 μT, respectively. These ranges support cooling at different periods. This study reports the first high quality archaeointensity data for northern Mexico.

4.3 *Archaeomagnetic dating*

Archaeomagnetic dating consists in the comparison of direction and/or intensity, obtained on a lava flow or an archaeological artefact of unknown age, with a reference PSV curve generated from a set of well-dated materials. The dating procedure is done by integrating, with a certain confidence level, probability density functions that obtained from comparing EMF elements (declination, inclination, or intensity) with their counterparts in the reference curve. Combining the density functions produces a unique date or a set of possible dates. For the latter, the most likely age may be assigned by using some independent details from the stratigraphic or archaeological background. In this study, the integration is done for intensity data, at a 95% confidence level. We used the MATLAB *archaeo_dating* software (Pavón-Carrasco et al., 2011). As the proposed archaeological age period for Mimbres and Ramos is 900–1450 AD, we restrict the dating analysis to 500-1600 AD.

In Mexico, as well as in American Southwest, most intensity data present in databases such as GEOMAGIA50 cannot be considered of high quality with our current quality standards (Hervé et al., 2019; Mahgoub et al., 2019a; Jones-Cervantes et al., 2020). That's why we choose to use the regional curve of Mahgoub et al. (2019a), and the SHAWQ2k global model (Campuzano et al., 2019) that both were built with a quality selected dataset. From here, we will refer to SHAWQ2k and Mahgoub curves as global and regional curves, respectively. Both curves have been generated at the coordinates of Mexico City (19.43º N, 99.13º W) and all archaeointensities have been also relocated there (Table 3), through virtual axial dipole moment (Creer et al., 1983). Of course, the regional and global curves could also have been relocated to Paquimé coordinates, however, we choose not to implement that option because of the absence of intensity data in northern Mexico.

The archaeomagnetic age ranges for each sherd (five for Mimbres and four for Ramos polychrome) are summarized in Table 4. Typical examples obtained with the regional and

301 global curves are presented in Figure 7 for each pottery type, and all archaeomagnetic dating
302 with the regional curve are listed in the supplementary material. The regional and the global
303 curves give very different age ranges (Table 4) but clearly those obtained with the regional
304 curve are in much better agreement with archeological estimations (1200-1450 AD for
305 Ramos and 1000-1150 AD for Mimbres). For Mimbres, regional-based age ranges are
306 usually pretty tight except for one sherd (VAM4, Figure 8), that gives a much larger range
307 because of its bimodal distribution (supp. material). Privileging the first mode makes the age
308 range for Mimbres much shorter, between 960-1100 AD. For Ramos, the age ranges are
309 slightly wider but in agreement between 1300-1600 AD.

310

311 **5. Discussion**

312 The precision of the obtained archeomagnetic ages depends on several factors, including (1)
313 the fidelity of the archaeointensity results; (2) the used reference curve; and (3) the relocation
314 approach. The archaeointensity data (Table 3) is of good quality after the anisotropy of
315 ATRM correction to all specimens. The cooling rate effect, however, could not be estimated
316 for each specimen and rather an average cooling-rate correction factor of 0.96 (estimated on
317 a few numbers of specimens from both Ramos and Mimbres types) was applied to all
318 specimens. We think that this limitation has little impact on our dating results.

319 Regarding the reference curves, archaeomagnetic dates derived from SHAWQ2k global
320 model (Campuzano et al., 2019) significantly differ from those obtained with Mahgoub et al.
321 (2019a) regional curve, the latter being more consistent with the archaeological context
322 (Table 4). The inaccuracy of SHAWQ2k model is likely attributed to the fact that it includes
323 Mexican intensity data without a reliable TRM anisotropy correction and without the cooling
324 rate correction, which yields to an overestimation of the geomagnetic field strength (Hervé
325 et al., 2019). In comparison, Mahgoub et al. (2019a) curve was constructed with a stricter
326 data selection, with more high-quality data (e.g. their new dataset) and after a revision of the
327 age of some previous data.

328 The precision of the relocation process depends on the magnitude of the non-dipole field
329 between Central and northern Mexico, but cannot be evaluated at that moment due to the lack
330 of intensity data in northern Mexico. According to Casas and Incoronato (2007), 1000 km

relocation can introduce an error of 1.5 μT on average. We do not insert an error to the relocated intensity values (Table 3), as we do not have precise information on the characteristics of the non-dipole field due to the lack of high-quality data in Mexico and the USA. After comparing the intensity curve for Central Mexico with southern USA curve, García et al. (2020) argued that non-dipole field between the two regions was small for the past two millennia. We cannot evaluate this suggestion for the moment, but it should be pointed that the data selection strategy used by García et al. (2020) includes data that were not considered of sufficient quality in previous studies (Hervé et al., 2019; Mahgoub et al., 2019a, 2019b; Jones-Cervantes et al., 2020).

Despite the mentioned uncertainties, archaeomagnetic dating was clearly able to discriminate between Mimbres and Ramos types and will then be extremely useful to precise the chronology of other not so easily identified sherds. We therefore recommend their use for future archaeological studies on the Casas Grandes culture. Obviously, new high-quality/well-dated palaeomagnetic data from northern Mexico will improve further the precision of the archaeomagnetic dating.

6. Conclusions

The reported archaeomagnetic results show that the magnetic and archaeointensity experiments can be used as proxies to differentiate between the Mimbres and Ramos ceramic types. Both sherd types were collected from four archaeological sites from Pre-Hispanic culture of Casas Grandes region: Paquimé; Villa Ahumada; Galeana; and Samalayuca, which has global archaeological age of 900–1450 AD. The archaeointensity values for Mimbres and Ramos types range between 49-59 μT and 41-49 μT, respectively. The difference between the archaeointensity values clearly demonstrates the non-contemporaneity of the two ceramic types. For dating purpose, the archaeointensity values were compared to global and regional secular variations curves for Central Mexico. Archaeomagnetic dating results at 95% of confidence are 960-1100 AD for Mimbres type and 1300-1600 AD for Ramos polychrome type. These dates are consistent with the archaeological context. Interestingly, the different magnetomineralogical properties of Mimbres and Ramos sherds indicate that the raw clay materials and probably the baking tradition used in the manufacturing process

were different at the two periods. This study confirms the ability of archaeomagnetism to date displaced archaeological materials in Central America and of rock magnetism to characterize and differentiate archaeological materials.

Acknowledgements

We thank the financial support for the research project DGAPA-PAPIIT-UNAM IN113117 to LA. We also thank the ANR-CONACyT 273564 to MP and LA (France-Mexico). AN Mahgoub and A Rodríguez-Trejo acknowledged the financial support of the Universidad Nacional Autónoma de México-postdoctoral fellowship at Geophysics Institute-UNAM, CDMX and Centro de Geociencias-UNAM, Querétaro, México, respectively. We thank the staff of the BCCT-UNAM (head, Saúl Armendariz) for their technical assistance.

References

Aitken, M.J., 1966. Magnetic field work. Archaeometry 9, 200–201. https://doi.org/10.1111/j.1475-4754.1966.tb00920.x.

Aitken, M.J., Alcock, P.A., Bussell, G.D., Shaw, C.J., 1981. Archeomagnetic determination of the past geomagnetic intensity using ancient ceramics: allowance for anisotropy. Archeometry, 23(1), 53-64.

Aitken M.J., Allsop, A.L., Bussell, G.D. et al., 1988. Determination of the intensity of the Earth's magnetic-field during archaeological times – Reliability of the Thellier technique. Reviews of Geophysics 26(1): 3–12.

Alva-Valdivia, L.M., Rodríguez-Trejo, A., Vidal-Solano, J.R., Paz-Moreno, F., Agarwal, A., 2019. Emplacement temperature resolution and age determination of Cerro Colorado tuff ring by TRM analysis, El Pinacate Volcanic Field, Sonora, Mexico. J. Volcanol. Geotherm. Res. 369, 145–154.

Arneitz, P., Egli, R., Leonhardt, R., Fabian, K., 2019. A Bayesian iterative geomagnetic model with universal data input: Self-consistent spherical harmonic evolution for the geomagnetic field over the last 4000 years. Physics of the Earth and Planetary Interiors, 290, 57–75. https://doi.org/10.1016/j.pepi.2019.03.008

Arrighi, S., Tanguy, J.-C., Rosi, M., 2006. Eruptions of the last 2200 years at Vulcano and Vulcanello (Aeolian Islands, Italy) dated by high-accuracy archaeomagnetism, Phys. Earth planet. Inter., 159, 225–233.

Bandelier, A.F., 1890. The Ruins of Casas Grandes. The Nation, 51(1313-1314), 166-168.

Bishop, R.L., 1992. Archeometry of pre-Columbian sites and artifacts, Proceedings of the Symposium organized by UCLA, Institute of Archeology and the Getty Conservation Institute, Los Angeles, California, 15–63.

Bishop, R.L., Blackman, M.J., 2002. Instrumental neutron activation analysis of archeological ceramics: scale and interpretation, Accounts of Chemical Research, 35(8), 603–610.

Böhnel, H., Pavón-Carrasco, F.J., Sieron, K., Mahgoub, A.N., 2016. Palaeomagnetic dating of two recent lava flows from Ceboruco volcano, western Mexico. Geophys. J. Int.207 (2), 1203–1215.

Brand, D.D., 1943. The Chihuahua culture area. New Mexico Anthropologist, 6(3), 115-158.

Braniff, C.B., 1986. Ojo de Agua, Sonora, and Casas Grandes, Chihuahua: A Suggested Chronology. Ripples in the Chichimec Sea, Southern Illinois University Press, Carbondale, 70-80.

Brown, M.C., Donadini, F., Korte, M., Nilsson, A., Korhonen, K., Lodge, A., ... & Constable, C. G., 2015. GEOMAGIA50. v3: 1. General structure and modifications to the archaeological and volcanic database. Earth, Planets and Space, 67(1), 83.

Campuzano, S.A., Gómez-Paccard, M., Pavón-Carrasco, F.J., Osete, M.L., 2019. Emergence and evolution of the South Atlantic Anomaly revealed by the new paleomagnetic reconstruction SHAWQ2k. Earth and Planetary Science Letters, 512, 17–26. https://doi.org/10.1016/j.epsl.2019.01.050

Carl, L., 1904. El Mexico desconocido: Cinco años de exploración entre las tribus de la Sierra Madre Occidental; en la tierra caliente de Tepic y Jalisco, y entre los tarascos de Michoacán. Instituto Nacional Indigenista, México.

Chauvin, A., Garcia, Y., Lanos, P., Laubenheimer, F., 2000. Paleointensity of the geomagnetic field recovered on archaeomagnetic sites from France. Phys Earth Planet Inter 120 (1–2), 111–136.

Coe, R.S., 1967. Palaeointensities of the Earth's magnetic field determined from tertiary and quaternary rocks. Journal of Geophysical Research-Solid Earth 72, 3247–3262.

Coe, R.S., Gromme, S., Mankinen, E.A., 1978. Geomagnetic paleointensities from radiocarbon-dated lava flows on Hawaii and the question of the Pacific nondipole low. J. Geophys. Res.83, 1740–1756.

Constable, C., Korte, M., Panovska, S., 2016. Persistent high paleosecular variation activity in southern hemisphere for at least 10 000 years. Earth and Planetary Science Letters, 453, 78-86.

Cordell, L.S., 1984. Prehistory of the Southwest. Academic Press.Cordell, L.S., & McBrinn, M. (2016). Archeology of the Southwest. Routledge.

Cox, J., & Blinman, E., 1999. Results of archeomagnetic sample analysis. Pipeline Archeology 1990e1993: The El Paso Natural Gas North System Expansion Project, New Mexico and Arizona, 12, 19-1.

Creer, K.M., Tucholka, P., Barton, C.E., 1983. Geomagnetism of Baked Clays and Re-cent Sediments. Elsevier, Amsterdam. 324 pp

Cruz Antillón, R., Maxwell, T.D., 1999. The Villa Ahumada Site: Archaeological Investigations East of Paquimé. The Casas Grandes World, 43-53.

Cruz Antillón, R., Maxwell, T.D., 2017. La Cultura Casas Grandes. Secretaría de Cultura, Instituto Nacional de Antropología e Historia, Gobierno del Estado de Chihuahua.

Day, R., Fuller, M., Schmidt, V.A., 1977. Hysteresis properties of titanomagnetites: grain-size and compositional dependence. Physics of the Earth and planetary interiors, 13(4), 260-267.

Dean, J.S., Ravesloot, J.C., 1993. The chronology of cultural interaction in the Gran Chichimeca. Culture and Contact: Charles C. Di Peso's Gran Chichimeca, 83-103.

De Marco, E., Spassov, S., Kondopoulou, D., Zananiri, I., Gerofoka, E., 2008. Archaeomagnetic study and dating of a Hellenistic site in Katerini (N. Greece). Phys. Chem.

448 Earth 33 (6), 481–495. https://doi.org/10.1016/j.pce.2008.02.017

449 Di Peso, C.C., 1965. The Clovis Fluted Point from the Timmy Site, Northwest
450 Chihuahua, Mexico. Kiva, 31(2), 83-87.

451 Di Peso, C.C., 1974a. Casas Grandes, vol. 1–3. Dragoon, Arizona: Amerind
452 Foundation.

453 Di Peso, C.C., 1974b. The Reeve ruin of Southeastern Arizona: A study of a
454 prehistoric western pueblo migration into the middle San Pedro valley (No. 8). Kraus Reprint
455 Company.

456 Di Peso, C.C., Fenner, G.J., Wesche, A., 1974. Casas Grandes: a fallen trading center
457 of the Gran Chichimeca (Vol. 8). Dragoon, AZ: Amerind Foundation.

458 Dodson, M.H., McClelland-Brown, E., 1980. Magnetic blocking temperatures of
459 singledomain grains during slow cooling. J. Geophys. Res. 85, 2625–2637.

460 Dunlop, D.J., 2002. Theory and application of the Day plot (Mrs/Ms versus Hcr/Hc)
461 2. Application to data for rocks, sediments, and soils. Journal of Geophysical Research: Solid
462 Earth, 107(B3), EPM-5.

463 Eighmy, J.L., Hathaway, T.K., Henderson, T.K., 1986. Secular change in the
464 direction of the geomagnetic field, AD 900 to 1100: new US southwest data. MASCA
465 journal, 4(2), 81-85.

466 Eighmy, J.L., R.S. Sternberg (Eds.), 1990, Archaeomagnetic Dating, 367–393 pp.,
467 Univ. of Ariz. Press, Tucson

468 Fanjat, G., Camps, P., Alva-Valdivia, L.M., Sougrati, M.T., Cuevas-Garcia, M.,
469 Perrin, M., 2013. First AI determinations on Maya incense burners from Palenque temples,
470 Mexico: New data to constrain the Mesoamerica secular variation curve. Earth and Planetary
471 Science Letters, 363, 168-180.

472 García, R., Pérez-Rodríguez, N., Goguitchaichvili , A., Rodríguez Ceja, M., Morales,
473 J., Maria Soler, A., Urrutia-Fucugauchi, J., 2020. On the absolute geomagnetic intensity
474 fluctuations in Mexico over the last three millennia. South American Earth Sciences. 102927.
475 https://doi.org/10.1016/j.jsames.2020.102927.

476 Goguitchaichvili, A., Morales, J., Aguayo Haro, R., Quiroz Castañon, H., Robles

Camacho, J., 2016. First evidence of complex dental practice about 1300 BP in Mesoamerica revealed by absolute geomagnetic intensity. Studia Geophys. Geod. 61. https:doi.org/10.1007/s11200-016-0851-3.

Goguitchaichvili, A., Ortega, V., Archer, J., Morales, J., Guerrero, A. T., 2017. Absolute geomagnetic intensity record from pre-Columbian pottery dates elite Tlailotlacan Woman in ancient Teotihuacan. Journal of Archaeological Science: Reports, 14, 146-151.

Goguitchaichvili, A., Ruiz, R.G., Pavón-Carrasco, F.J., Contreras, J.J.M., Arechalde, A.M.S., & Urrutia-Fucugauchi, J., 2018. Last three millennia Earth's Magnetic field strength in Mesoamerica and southern United States: Implications in geomagnetism and archeology. Physics of the Earth and Planetary Interiors, 279, 79-91.

Hagstrum, J.T. Blinman, E., 2010. Archeomagnetic dating in western North America: an updated reference curve based on paleomagnetic and archeomagnetic data sets, Geochem. Geophys. Geosyst., 11, Q06009, doi:10.1029/2009GC002979.

Hagstrum, J.T., Champion, D.E., 2002. A Holocence geomagnetic secular variation record from 14C-dated volcanic rocks in Western America. J. Geophs. Res. 107 (B1), 2025. doi:10.1029/102001/JB000524.

Halgedhal, S., Day, R., Fuller, M., 1980. The effect of the cooling rate on the intensity of weak field TRM in single domain magnetite. J. Geophys. Res. 85, 3690–3698.Hegmon, M., Nelson, M. C., Anyon, R., Creel, D., LeBlanc, S. A., & Shafer, H. J. (1999). Scale and time-space systematics in the post-AD 1100 Mimbres region of the North American Southwest. Kiva, 65(2), 143-166.

Hellio, G., Gillet, N., 2018. Time-correlation-based regression of the geomagnetic field from archeological and sediment records. Geophysical Journal International, 214, 1585–1607. https://doi.org/10.1093/gji/ggy214

Hervé, G., Fassbinder, J., Gilder, S.A., Metzner-Nebelsick, C., Gallet, Y., Genevey, A., Schnepp, E., Geisweid, L., Pütz, A., Reuss, S., Wittenborn, F., Flontas, A., Linke, R., Riedel, G., Walter, F., Westhausen, I., 2017. Fast geomagnetic field intensity variations between 1400 and 400 BCE: new archaeointensity data from Germany. Phys. Earth Planet. Inter. 270, 143–156. https://doi.org/10.1016/j.pepi.2017.07.002.

Hervé, G., Lanos, P., 2018. Improvements in archaeomagnetic dating in Western Europe from the Late Bronze to the Late Iron ages: an alternative to the problem of the Hallstattian radiocarbon plateau. Archaeometry 60 (4), 870–883.

Hervé, G., Perrin, M., Alva-Valdivia, L., Tchibinda, B.M., Rodriguez-Trejo, A., Hernandez-Cardona, A., Cordova-Tello, M., Rodriguez, C.M., 2019. Critical analysis of the Holocene palaeointensity database in Central America: Impact on geomagnetic modelling. Physics of the Earth and Planetary Interiors, 289, 1-10.

Isabella, J., 2013. On the trail of the Mimbres. Archaeology, May-June.

Kelley, J.H., Phillips, D.A., 2017. Not so far from Paquimé: essays on the archeology of Chihuahua, Mexico. University of Utah Press.

Kelley, J.H., Searcy, M.T., 2015. Beginnings: The Viejo Period. Ancient Paquimé and the Casas Grandes World, 17-40. Eds. Paul E Minnis and Michael E. Whalen, pp. 17-40. Amerind Studies in Anthropolgy, The University of Arizona Press, Tucson.

Kelley, J.H., Garvin, R.D., Stewart, J.D., Zborover, D., Chiykowski, T., 2014. The Viejo Period in West-Central Chihuahua, Part 2: The Calderón site. In Maxwell Museum Technical Series No. 19, Part 2. Maxwell Museum of Anthropology, University of New Mexico Albuquerque.

Kirchhoff, P., 1954. Gatherers and farmers in the Greater Southwest: a problem in classification. American Anthropologist, 56(4), 529-550.

Kirschvink, J.L., 1980. The least-squares line and plane and analysis of palaeomag-netic data. Geophys. J. R. Astron. Soc.62, 699–718.

Korte, M., Constable, C., Donadini, F., Holme, R., 2011. Reconstructing the Holocene geomagnetic field. Earth and Planetary Science Letters, 312(3-4), 497-505.

Korte, M., Donadini, F., Constable, C.G., 2009. Geomagnetic field for 0–3 ka: 2. A new series of time-varying global models. Geochemistry, Geophysics, Geosystems, 10(6).

Kovacheva, M., Kostadinova-Avramova, M., Jordanova, N., Lanos, P., Boyadzhiev, Y., 2014. Extended and revised archaeomagnetic database and secular variation curves from Bulgaria for the last eight millennia. Phys. Earth Planet. Inter.236, 79–94. https://doi .org /10 .1016 /j .pepi .2014 .07.002.

Lengyel, S.N., Eighmy, J.L., 2002. A revision to the US Southwest archeomagnetic master curve. Journal of archaeological science, 29(12), 1423-1433.

Lengyel, S.N., Eighmy, J.L., Sullivan, L.P., 1999. On the potential of archeomagnetic dating in the midcontinent region of North America: Toqua site results. Southeastern Archeology, 156-171.

Leonhardt, R., Soffel, H.C., 2002. A reversal of the Earth's magnetic field recorded in mid-Miocene lava flows of Gran Canaria: Paleointensities, J. Geophys. Res., 107(B11), 2299, doi:10.1029/2001JB000949.

Leonhardt, R., Heunemann, C., Krása, D., 2004. Analyzing absolute paleointensity determinations: Acceptance criteria and the software ThellierTool4. 0. Geochemistry, Geophysics, Geosystems, 5(12).

Mahgoub, A.N., Reyes-Guzmán, N., Böhnel, H., Siebe, C., Pereira, G., Dorison, A., 2018. Paleomagnetic constraints on the ages of the Holocene Malpaís de Zacapu lava flow eruptions, Michoacán (México): Implications for archeology and volcanic hazards. Holocene. https://doi.org/10.1177/0959683617721323.

Mahgoub, A.N., Böhnel, H., Siebe, C., Chevrel, M.O., 2017. Paleomagnetic study of El Metate shield volcano (Michoacán, Mexico) confirms its monogenetic nature and young age (~1250 CE). J. Volcanol. Geotherm. Res.336, 209–218. https://doi .org /10 .1016 /j .ejvolgeores .2017.02 .024.

Mahgoub, A.N., Juárez-Arriaga, E., Böhnel, H., Siebe, C., Pavón-Carrasco, F.J., 2019a. Late-Quaternary secular variation data from Mexican volcanoes. Earth and Planetary Science Letters, 519, 28-39.

Mahgoub, A.N., Juárez-Arriaga, E., Böhnel, H., Manzanilla, L.R., Cyphers, A., 2019b. Refined 3600 years palaeointensity curve for Mexico. Phys. Earth Planet. In. 296. https://doi.org/10.1016/j.pepi.2019.106328.

Mathiowetz, M.D., 2019. A history of Cacao in West Mexico: implications for Mesoamerica and U.S. Southwest Connections. J. Archaeol. Res.

Morales, J., Goguitchaichvili, A., Acosta, G., González-Moran, T., Alva-Valdivia, L., Robles-Camacho, J., & del Sol Hernández-Bernal, M., 2009. Magnetic properties and AI

564 determination on Pre-Columbian pottery from Chiapas, Mesoamerica. Earth, planets and
565 space, 61(1), 83-91.

566 Nagata, T., Kobayashi, K., Schwarz, E.J., 1965. Archeomagnetic intensity studies of
567 South and Central America. J. Geomagn. Geoelectr.17, 399–405.

568 Oppelt, N.T., 2002. List of Southwestern Pottery: Types and Wares: with Dates and
569 References to Descriptions and Illustrations. Oppelt Publications.

570 Pailes, M., 2017. Northwest Mexico: The prehistory of Sonora, Chihuahua, and
571 neighboring areas. Journal of Archaeological Research 25: 373–420.

572 Parada Carrillo, G., 2016. Arquitectura y cerámica de Casas Grandes. Una
573 comparación entre conceptos espaciales arquitectónicos y pictóricos. In Anales del Instituto
574 de Investigaciones Estéticas (Vol. 38, No. 109, pp. 171-214). Universidad Nacional
575 Autónoma de México, Instituto de Investigaciones Estéticas.

576 Paterson, G.A., Tauxe, L., Biggin, A.J., Shaar, R., Jonestrask, L.C., 2014. On
577 improving the selection of Thellier-type paleointensity data. Geochemistry, Geophysics,
578 Geosystems, 15(4), 1180-1192.

579 Pavón-Carrasco, F.J., Osete, M.L., Torta, J.M., De Santis, A., 2014. A geomagnetic
580 field model for the Holocene based on archeomagnetic and lava flow data. Earth and
581 Planetary Science Letters, 388, 98-109.

582 Pavón-Carrasco, F.J., Rodríguez-González, J., Osete, M.L., Torta, J.M., 2011. A
583 Matlab tool for archeomagnetic dating. Journal of Archaeological Science, 38(2), 408-419.

584 Ravesloot, J.C., Dean, J.S., Foster, M.S., 1986. A new perspective on the Casas
585 Grandes tree-ring dates. In Fourth Mogollon Conference, University of Arizona.

586 Ravesloot, J.C., Dean, J.S., Foster, M.S., 1986. A new perspective on the Casas
587 Grandes tree-ring dates. In Fourth Mogollon Conference, University of Arizona.

588 Rogers, J., Fox, J.M.W., Aitken, M.J., 1979. Magnetic anisotropy in ancient pottery.
589 Nat. 277, 644–646.

590 Rodriguez-Trejo, A., Alva-Valdivia, Vidal-Solano., 2019a. Paleomagnetism and rock
591 magnetic properties of Late Pleistocene volcanism from El Pinacate Volcanic Field,
592 northwest Mexico. Journal of South American Earth Sciences.

https://doi.org/10.1016/j.jsames.2019.102368.

Rodriguez-Trejo, A., Alva-Valdivia, L. M., Perrin, M., Hervé, G. and Lopez-Valdes, N., 2019b. Analysis of geomagnetic secular variation for the last 1.5Ma recorded by volcanic rocks of the TransMexican Volcanic Belt: new data from Sierra de Chichinautzin, Mexico. Geophys. J. Int., doi: 10.1093/gji/ggz310.

Roberts, A.P., Tauxe, L., Heslop, D., Zhao, X., Jiang, Z., 2018. A critical appraisal of the Day diagram. J. Geophys. Res. 123, 2618–2644. https://doi.org/10.1002/ 2017JB015247.

Sayles, E.B., 1936. An archaeological survey of Chihuahua, Mexico (No. 22). Priv. print. for the Medallion, Gila pueblo.

Schnepp, E. and Brüggler, M., 2016. Archaeomagnetic investigation of a Roman glass workshop in Goch-Asperden, Germany. Journal of Archaeological Science: Reports 10, 322-330.

Sternberg, R.S., 2008. Archaeomagnetism in archaeometry— a semi-centennial review. Archaeometry 50, 983–998. https://doi.org/10.1111/j.1475-4754.2008.00444.x.

Stewart, J.D., Kelley, J.H., MacWilliams, A.C., Reimer, P.J., 2005. The Viejo period of Chihuahua culture in northwestern Mexico. Latin American Antiquity, 16(2), 169-192.

Stewart, J.D., MacWilliams, A.C., Kelley, J.H., 2004. Archaeological Chronology in West-Central Chihuahua. Surveying the Archeology of Northwest Mexico, edited by Gillian E. Newell and Emiliano Gallaga, 205-245.

Tauxe, L., Bertram, H. N., Seberino, C., 2002. Physical interpretation of hysteresis loops: Micromagnetic modeling of fine particle magnetite. Geochemistry, Geophysics, Geosystems, 3(10), 1-22.

Tauxe, L., Mullender, T.A.T., Pick, T., 1996. Potbellies, wasp-waists, and superparamagnetism in magnetic hysteresis. Journal of Geophysical Research: Solid Earth, 101(B1), 571-583.

Tauxe, L., Staudigel, H., 2004. Strength of the geomagnetic field in the Cretaceous Normal Superchron: new data from submarine basaltic glass of the Troodos Ophiolite. Geochem. Geophys. Geosyst. 5 (Q02H06

Tema, E. Ferrara, E. Angelici, D., Fantino, F., Panero, E., 2019. The importance of

multidisciplinary dating in rescue excavations: The case of Santhià, Northern Italy. J. Archaeological Sci. Rep., v. 28, https://doi.org/10.1016/j.jasrep.2019.102059

Tema, E., Lanos,P., 2020. New Italian directional and intensity archaeomagnetic reference curves for the past 3000 years: insights on secular variation and implications on dating. Archaeometry. doi: 10.1111/arcm.12603

Thellier, E., Thellier, O., 1959. Sur l'intensité du champ magnétique terrestre dans le passé historique et géologique. Ann. Geophys.15, 285–376.

Thébault, E., Gallet, Y., 2010. A bootstrap algorithm for deriving the archeomagnetic field intensity variation curve in the Middle East over the past 4 millennia BC. Geophys. Res. Lett. 37, L22303. https://doi.org/10.1029/2010GL044788.

Valet, J.-P., J. Brassart, I. Le Meur, V. Soler, X. Quidelleur, E. Tric, and P.-Y. Gillot, 1996. Absolute paleointensity and magnetomineralogical changes, J. Geophys. Res., 101, 25,029–25,044.

VanPool, C.S., VanPool, T.L., 2007. Signs of the Casas Grandes shamans. University of Utah Press.

Veitch, R.J., 1984. An investigation of the intensity of the geomagnetic field during Roman times using magnetically anisotropic bricks and tiles. Arch. Sci. Geneve., 37(3), 359-373.

Whalen, M.E., Minnis, P.E., 2001. Casas Grandes and its hinterland: Prehistoric regional organization in northwest Mexico. University of Arizona Press.

Whalen, M.E., Minnis, P.E., 2009. The neighbors of Casas Grandes: excavating medio period communities of northwest Chihuahua, Mexico. University of Arizona Press.

Whalen, M.E., Minnis, P.E., 2012. Ceramics and polity in the Casas Grandes area, Chihuahua, Mexico. American Antiquity, 77(3), 403-423.

Wolfman, D., Eighmy, J.L., Sternberg, R. S., 1990. Archaeomagnetic dating. Archeomagnetic Dating, 237.

Figure caption

Figure 1. Location map of the sampling area shows Casas Grandes cultural region (pink area) and studied archaeological sites (red points).

Figure 2. Representative sample sherds from this study in the Casas Grandes region: Ramos polychrome, PR and Mimbres, PM. On the right, is shown typical example of Ramos polychrome (above, Parada-Carrillo, 2016) and Mimbres pottery (below, Isabella, J., 2013); scale is 30 cm wide.

Figure 3. Representative k-T curves of Ramos polychrome and Mimbres ceramic types from the distinct localities. In each graph, the calculated Curie temperature is indicated as circle.

Figure 4. Representative hysteresis curves from the different localities before and after subtraction of the paramagnetic components (in red and blue respectively). IRM and backfield curves are in the inset of each graph.

Figure 5. Day plot of samples from Ramos polychrome and Mimbres ceramic types with SD-MD mixing curves of Dunlop (2002).

Figure 6. Representative archaeointensity results with Arai plots to the left and orthogonal vector plots to the right. NRM vs. pTRM data are shown as red circles, with best-fit lines marked in dashed blue lines. pTRM checks are shown as triangles and some temperature steps are also indicated. Orthogonal vector plot: Black and white circles represent the projection of the magnetic vectors on the horizontal and vertical plane, respectively. Labels along curves denote the temperature steps during the intensity experiments

Figure 7. Typical archaeomagnetic dating results for Mimbres (a, b) and Ramos polychrome

(c, d) ceramic types using the regional (a, c) and global curves (b, d). The comparison of the average archaeointensity relocated to Mexico City with the curves provides the probability density function, on which are defined the intervals of date at 95% of confidence. * Selected interval according to the archaeological context.

Figure 8. Summary of archaeomagnetic dating results obtained with the regional curve for Mimbres and Ramos. The location of the diamonds on the range corresponds to the maximum of the probability distribution.

Table caption

Table 1. Location of the archaeological sites and acronyms of the sampled sherds

Table 2. Hysteresis parameters obtained in this study. M_{rs}, saturation remanent magnetization; M_s, saturation magnetization; H_c, coercive force; H_{cr}, remanent coercive force: M_{rs}/M_s, remanence ratio; H_{CR}/H_C, coercivity ratio.

Table 3. Summary of the archaeointensity results, obtained at specimen, sherd and pottery type levels.

Specimen name, locality and type; N: Number of temperature steps included in the best-fit line; f: NRM fraction; g: Gap factor; q: Quality factor; β: ratio of the standard error of the slope of the selected segment in the Arai plot to absolute value of the slope; d(CK): relative check error; d(Pal): cumulative check difference; α: angular difference between anchored and non-anchored best fit direction; MAD_{anc}: anchored maximum angular deviation; $F_{raw} \pm \sigma_F$: raw archaeointensity value with its standard deviation, calculated at each corresponding archaeological site coordinates (see Table 1); F_{ATRM}: archaeointensity values corrected for anisotropy of thermal remanent magnetization; $F_{ATRM+CR}$: archaeointensity value calculated after anisotropy and cooling rate corrections (4% cooling rate factor is constantly applied to all specimens); F (at C. Mexico): archaeointensity value relocated to Mexico City (19.43°N;

706 99.13°W); VADM: virtual axial dipole moment. Relocated F and VADM are calculated from
707 corrected archaeointensity values.

708

709 Table 4. Archaeomagnetic dating results obtained with regional curve for central Mexico
710 (Mahgoub et al., 2019a) and with the prediction of intensity values of SHAWQ2k global
711 model (Campuzano et al., 2019).

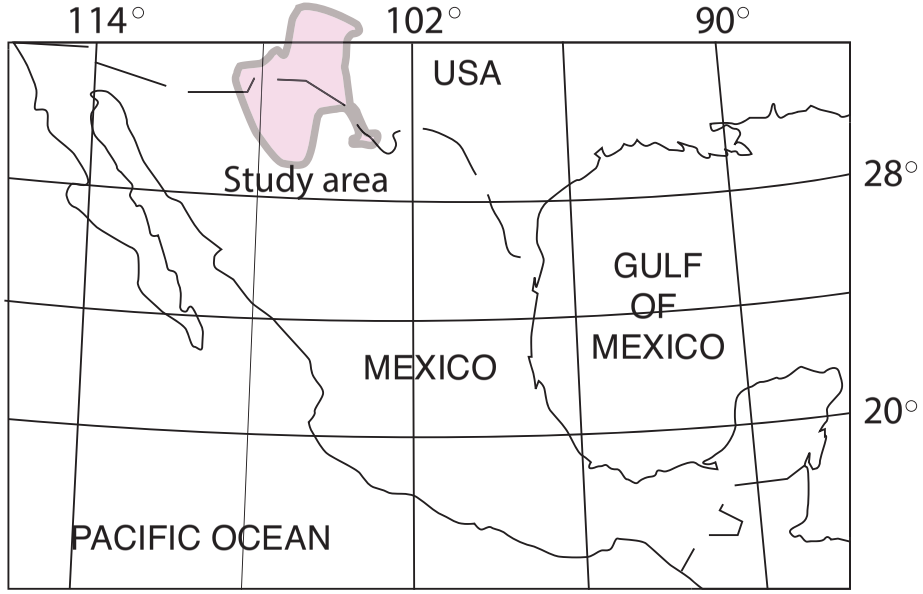
114°
102°
90°
USA
Study area
28°
GULF
OF
MEXICO
MEXICO
20°
PACIFIC OCEAN


Samalayuca
Villa Ahumada
Paquimé
Galeana
Chihuahua city

Figure 1

PR-1

PR-3

PM-1

1 cm

PR-7

PR-6

PM-2

Figure 3

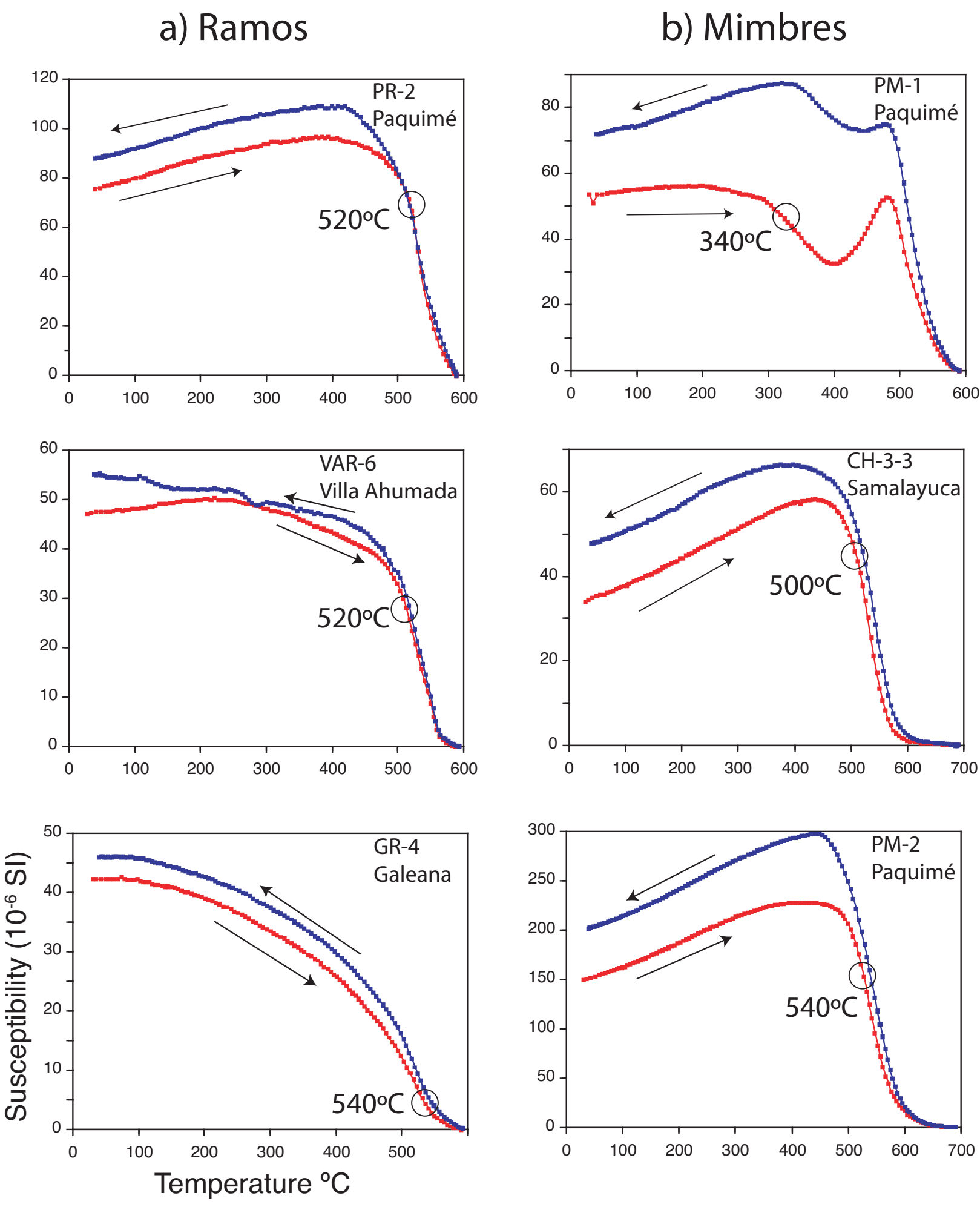
a) Ramos
b) Mimbres
PR-2
Paquimé
520ºC
PM-1
Paquimé
340ºC
VAR-6
Villa Ahumada
520ºC
CH-3-3
Samalayuca
500ºC
GR-4
Galeana
540ºC
PM-2
Paquimé
540ºC
Susceptibility (10-6 SI)
Temperature ºC

Figure 4

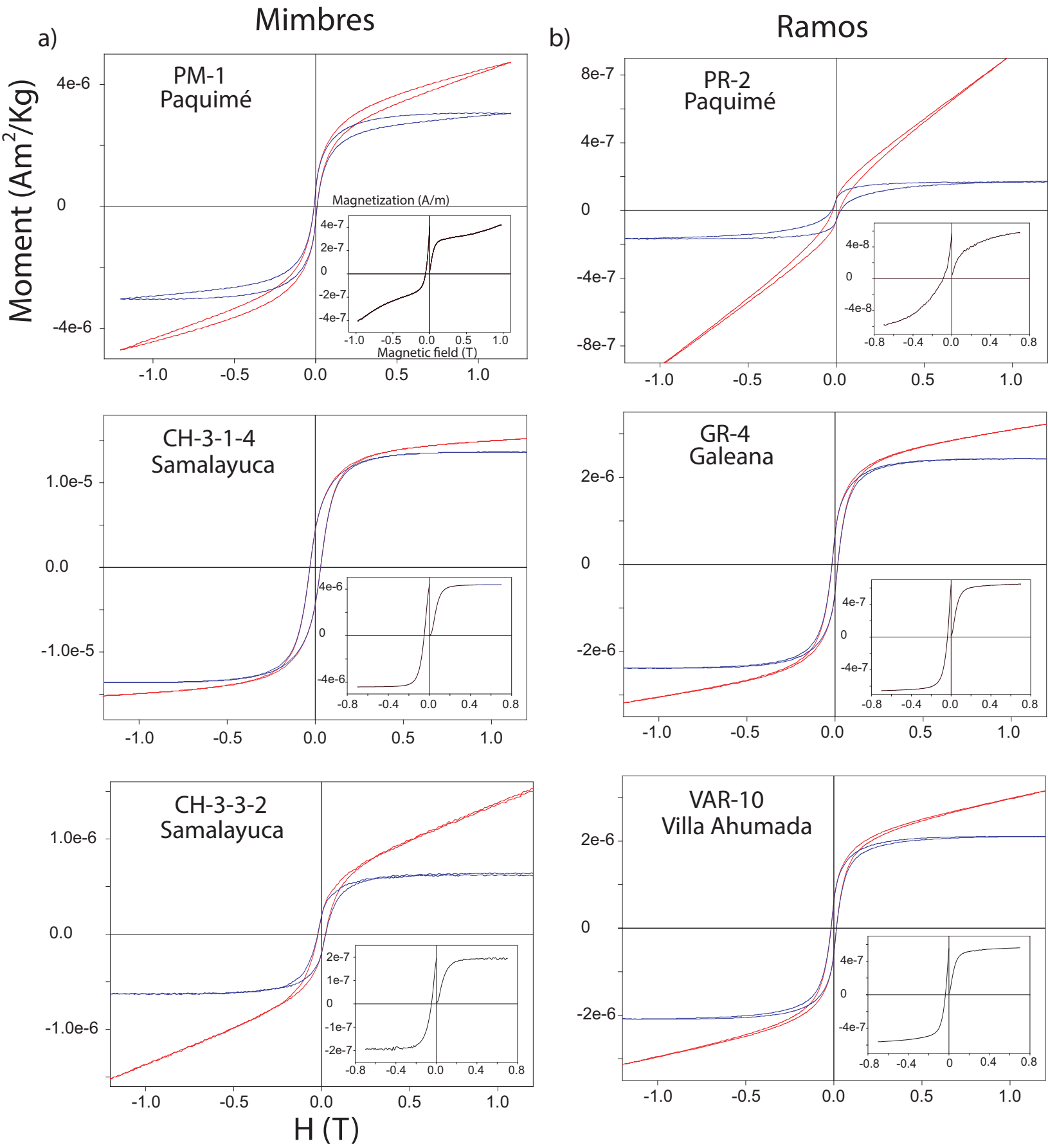
Mimbres
Ramos
a)
b)
Moment (Am²/Kg)
PM-1
Paquimé
Magnetization (A/m)
Magnetic field (T)
PR-2
Paquimé
CH-3-1-4
Samalayuca
GR-4
Galeana
CH-3-3-2
Samalayuca
VAR-10
Villa Ahumada
H (T)

Figure 5

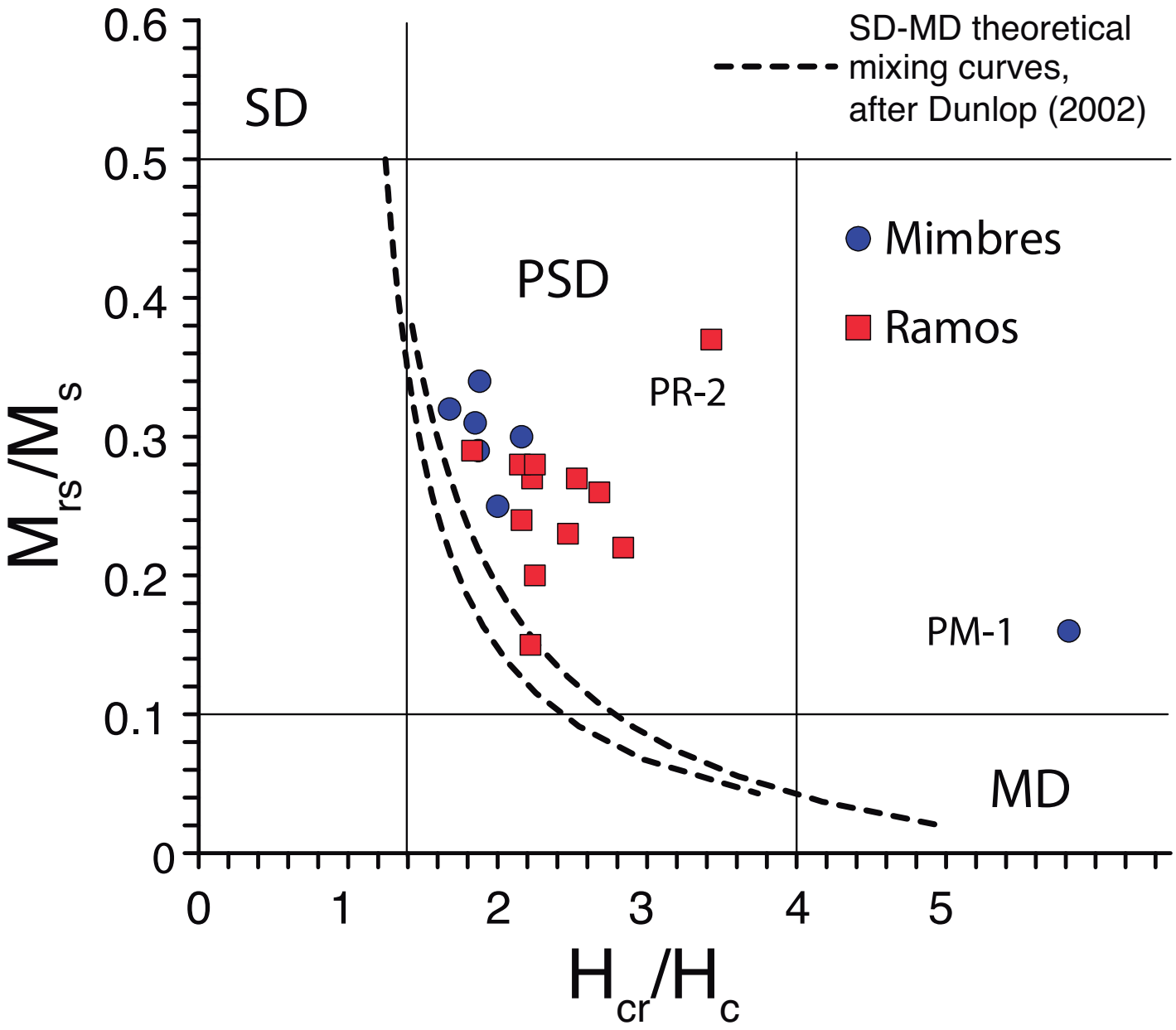
SD
PSD
MD
SD-MD theoretical
mixing curves,
after Dunlop (2002)
Mimbres
Ramos
PR-2
PM-1
0.6
0.5
0.4
0.3
0.2
0.1
0
0
1
2
3
4
5
M_{rs}/M_s
H_{cr}/H_c

Figure 6

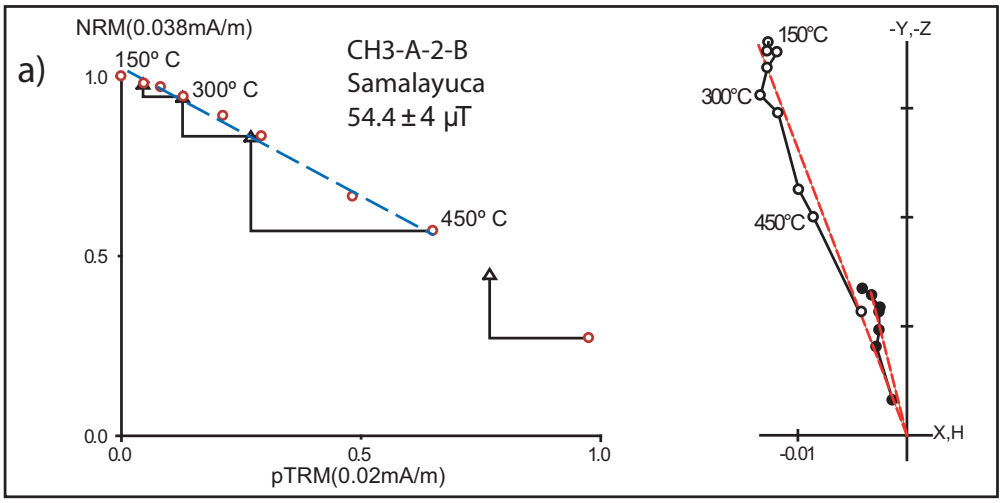
a)
NRM(0.038mA/m)
150° C
300° C
450° C
CH3-A-2-B
Samalayuca
54.4 ± 4 µT
1.0
0.5
0.0
0.0
0.5
1.0
pTRM(0.02mA/m)
150°C
300°C
450°C
-Y,-Z
X,H
-0.01

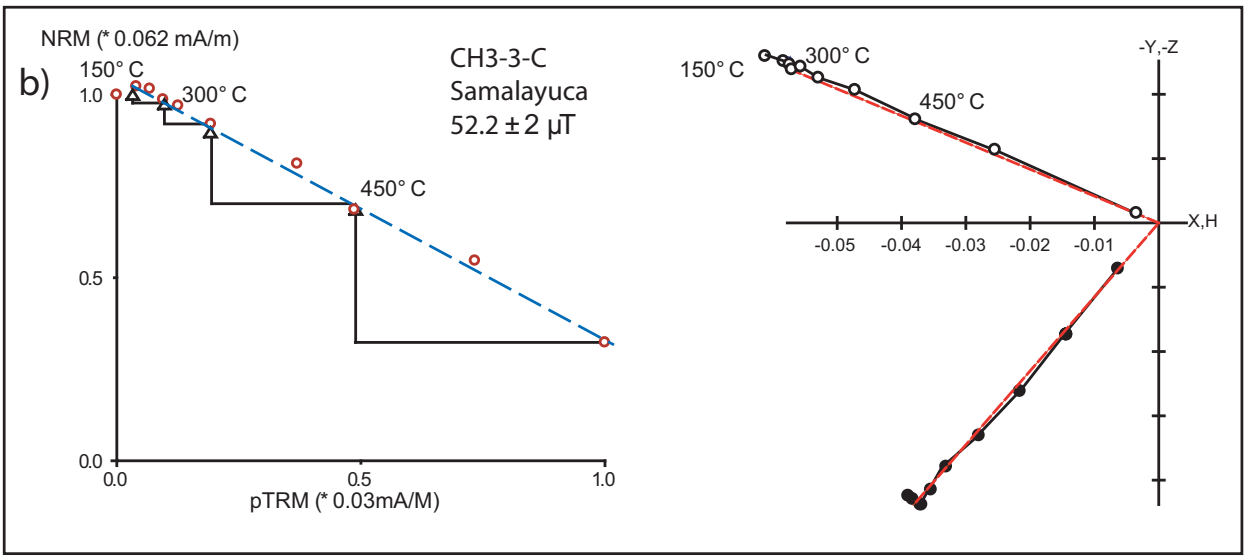
b)
NRM (* 0.062 mA/m)
150° C
300° C
450° C
CH3-3-C
Samalayuca
52.2 ± 2 µT
1.0
0.5
0.0
0.0
0.5
1.0
pTRM (* 0.03mA/M)
150° C
300° C
450° C
-Y,-Z
X,H
-0.05
-0.04
-0.03
-0.02
-0.01

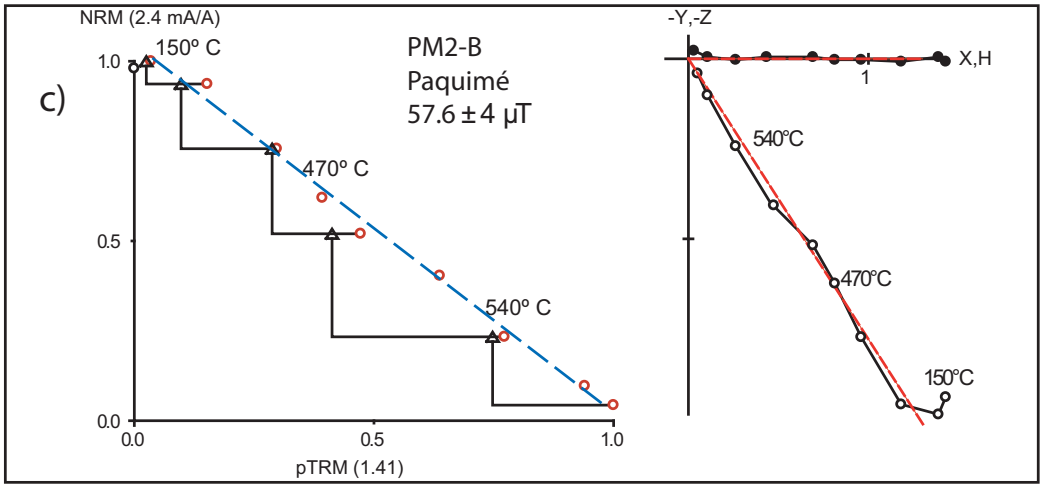
c)
NRM (2.4 mA/A)
150° C
470° C
540° C
PM2-B
Paquimé
57.6 ± 4 µT
1.0
0.5
0.0
0.0
0.5
1.0
pTRM (1.41)
-Y,-Z
X,H
1
540°C
470°C
150°C

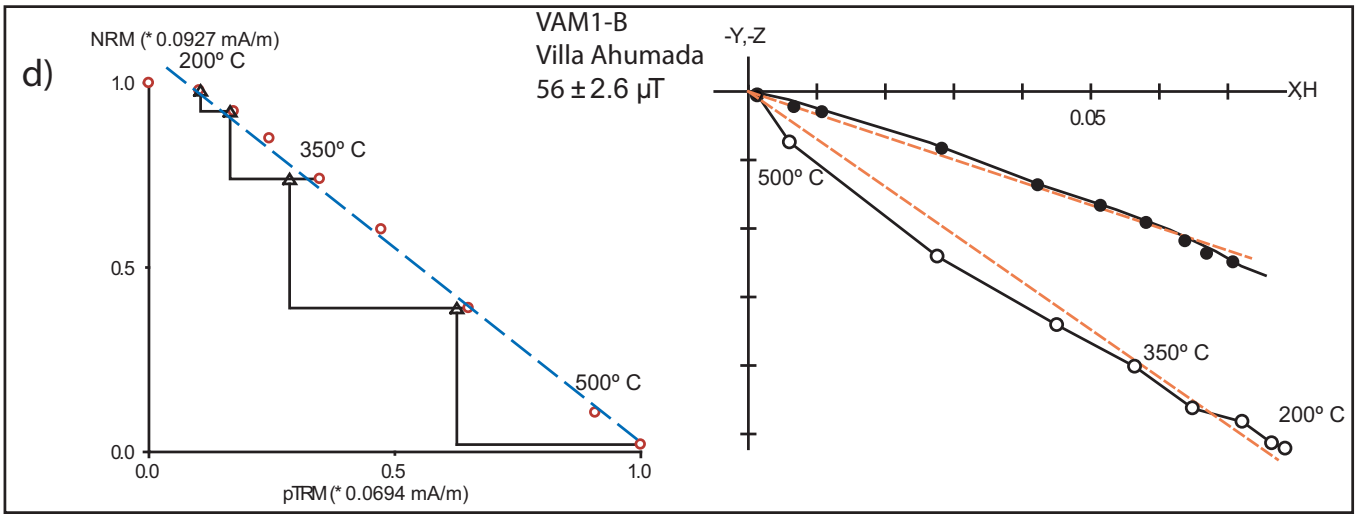
d)
NRM (* 0.0927 mA/m)
200° C
350° C
500° C
VAM1-B
Villa Ahumada
56 ± 2.6 µT
1.0
0.5
0.0
0.0
0.5
1.0
pTRM (* 0.0694 mA/m)
-Y,-Z
X,H
0.05
500° C
350° C
200° C

Figure 7

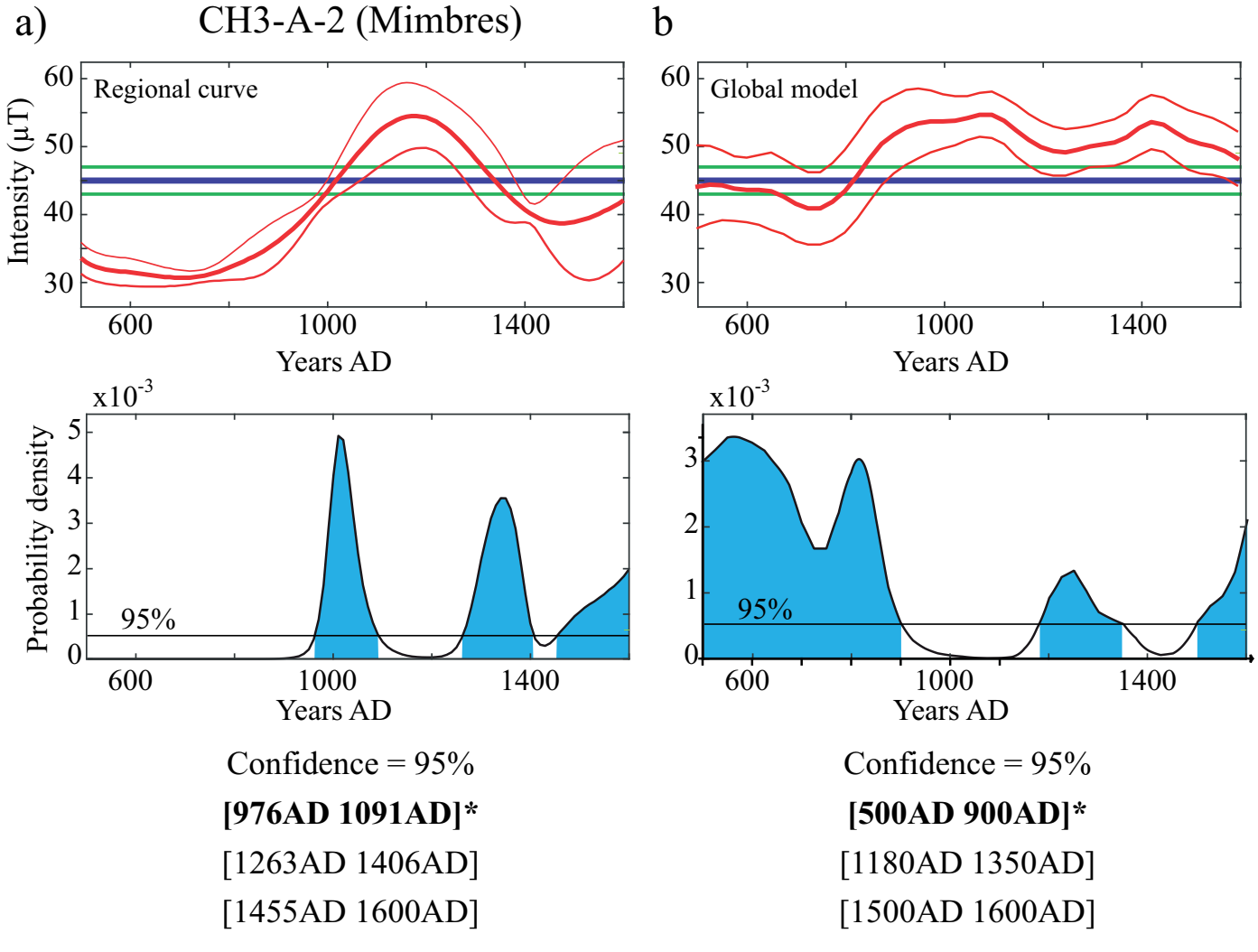

Confidence = 95%
[976AD 1091AD]*
[1263AD 1406AD]
[1455AD 1600AD]

Confidence = 95%
[500AD 900AD]*
[1180AD 1350AD]
[1500AD 1600AD]

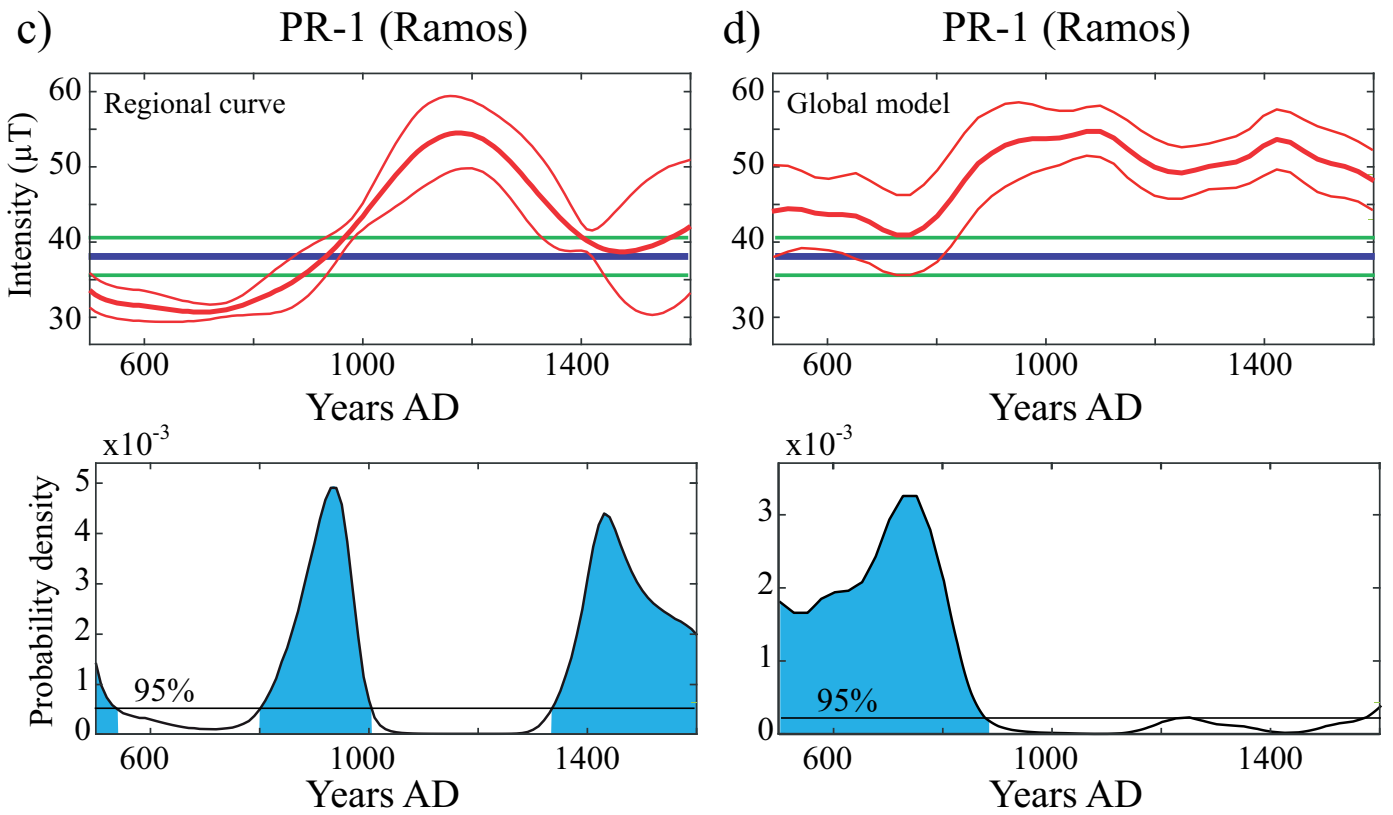

Confidence = 95%
[500AD 539AD]
[800AD 1004AD]
[1335AD 1600AD]*

Confidence = 95%
[500AD 880AD]*

Figure 8

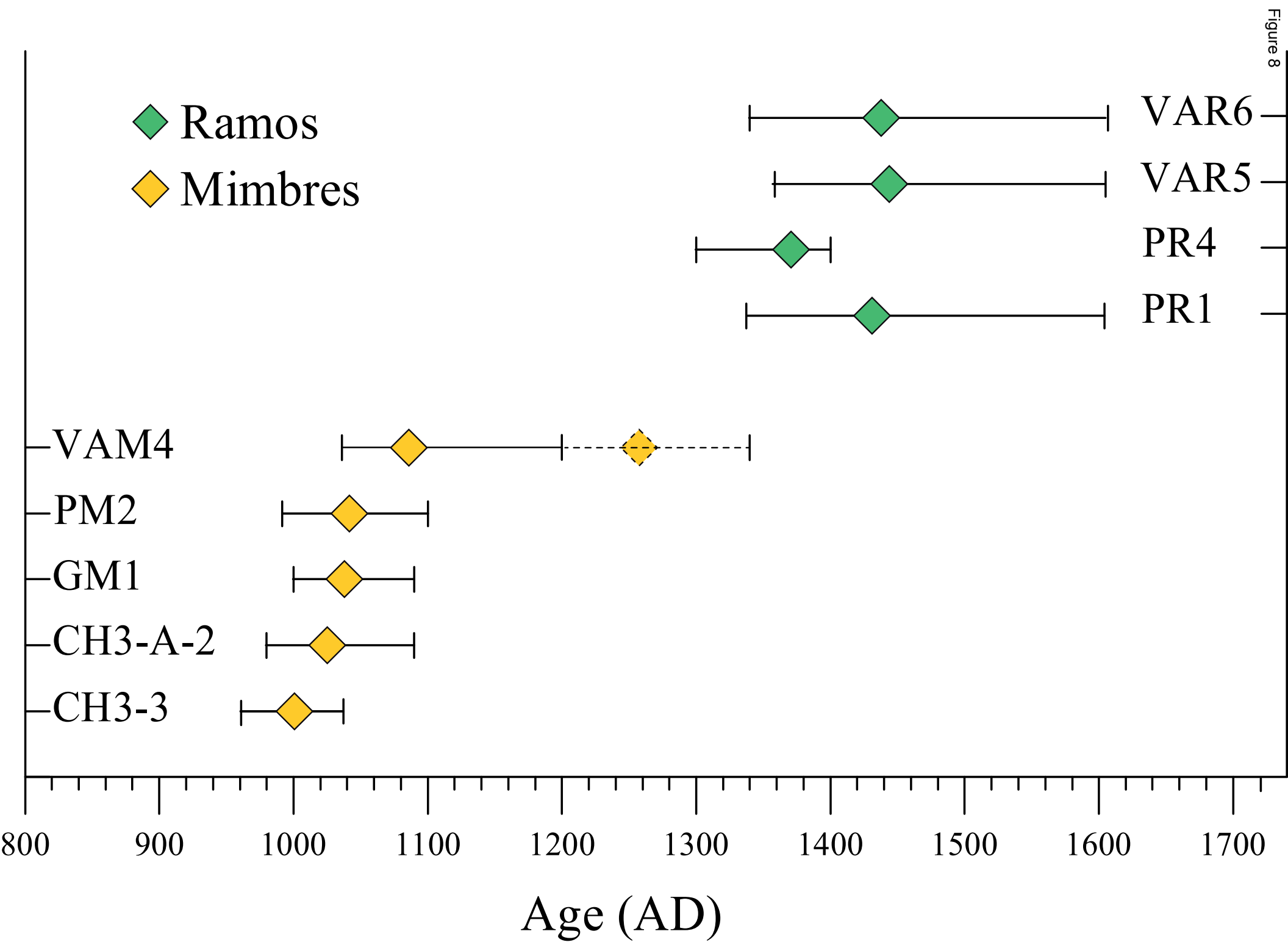
Ramos
Mimbres
VAR6
VAR5
PR4
PR1
VAM4
PM2
GM1
CH3-A-2
CH3-3
800
900
1000
1100
1200
1300
1400
1500
1600
1700
Age (AD)

Table 1

Archaeological site	*Location*		*Sherd names*
	Latitude °N	*Longitude °W*	
Paquimé	30.3674	107.9485	PM & PR
Samalayuca	31.3424	106.4309	CH
Villa Ahumada	30.6165	106.5228	VAM & VAR
Galeana	30.1079	107.6116	GM & GR

Table 2

Specimen	*Ceramic Type*	*Mrs*	*Ms*	*Hc*	*Hcr*	*Mrs/Ms*
Allan-p	Mimbres	62.01	217.1	28.22	52.83	0.29
CH-3-1-4	Mimbres	220.3	686.8	30.45	51.15	0.32
Ch-3-3-1	Mimbres	23.27	67.5	31.79	59.71	0.34
Ch-3-3-2	Mimbres	5.942	19.63	22.75	49.21	0.30
PM-1	Mimbres	18.17	113.6	9.711	56.52	0.16
VAM-1	Mimbres	26.13	104.6	23.54	47.16	0.25
VAM-4	Mimbres	16.1	52.55	29.55	54.75	0.31
GR-1	Ramos	41.21	173.2	20.82	44.87	0.24
GR-4	Ramos	26.74	99.18	16.63	37.04	0.27
GR-6	Ramos	18.5	92.68	12.27	27.62	0.20
GR-7	Ramos	38.58	133.1	12.61	23.03	0.29
GR-8	Ramos	17.93	66.37	18.3	46.3	0.27
PR-1	Ramos	14.14	50.46	13.91	29.84	0.28
PR-2	Ramos	2.021	5.461	25.94	88.92	0.37
PR-3	Ramos	1.431	6.149	19.27	47.67	0.23
PR-7	Ramos	14.71	98.66	7.92	17.6	0.15
VAR-7	Ramos	5.356	20.36	14.77	39.54	0.26
VAR-8	Ramos	11.52	53	10.64	30.17	0.22
VAR-10	Ramos	19.26	69.18	15.58	35.1	0.28

Hcr/Hc
1.87
1.68
1.88
2.16
5.82
2.00
1.85
2.16
2.23
2.25
1.83
2.53
2.15
3.43
2.47
2.22
2.68
2.84
2.25

Table 3

Table 3: Accepted archaeointensity results

Specimen	Locality	Type	N	Range °C	f	g	q	β	d(CK)	d(Pal)	α (°)	MAD_{anc} (°)	F_{raw}± σ_F (μT)	F_{ATRM} (μT)	$F_{ATRM+CR}$ (μT)	$F_{(ATRM+CR)}$ (Mexico city) (μT)	$VADM_{(ATRM+CR)}$ ($x10^{22}$ Am^2)
CH3-3-A	Samalayuca	Mimbres	10	20-530	0.8	0.8	9.3	0.065	8.82	8.13	7.9	7.14	51.5±3.3	51.0	49.0		
CH3-3-B	Samalayuca	Mimbres	10	250-530	0.8	0.8	16.0	0.039	6.91	7.97	4.36	3.86	51.8±2.0	50.3	48.3		
CH3-3-C	Samalayuca	Mimbres	10	250-530	0.7	0.8	14.6	0.085	4.98	6.44	3.54	4.1	52.2±2.0	50.7	48.7		
CH3-3-D	Samalayuca	Mimbres	10	20-570	1.0	0.8	41.4	0.020	7.06	9.38	1.15	3.21	51.8±1.0	50.3	48.3		
Sherd-mean													**51.8±0.3**	**50.6±.3**	**48.6±0.3**	**41.7±0.3**	**9.3**
CH3-A-2-A	Samalayuca	Mimbres	10	20-530	0.7	0.8	7.4	0.070	2.74	5.71	9.67	3.82	56.3±3.9	55.6	53.4		
CH3-A-2-B	Samalayuca	Mimbres	8	20-450	0.4	0.8	5.8	0.073	2.77	5.99	4.45	1.83	54.4±4.0	54.4	52.2		
CH3-A-2-C	Samalayuca	Mimbres	9	300-520	0.8	0.8	4.9	0.136	6.62	5.76	3.44	4.9	56.1±9.9	56.1	53.9		
CH3-A-2-D	Samalayuca	Mimbres	10	20-530	0.8	0.8	9.2	0.087	6.62	5.76	3.44	4.9	50.1±3.3	50.1	48.1		
Sherd-mean													**54.2±2.9**	**54.1±2.7**	**51.9±2.6**	**44.5±2.2**	**10.0**
GM1-A	Galeana	Mimbres	7	330-480	0.4	0.8	4.7	0.093	8.82	10.12	7.9	6.14	55.7±3.9	54.6	52.4		
GM1-B	Galeana	Mimbres	9	20-540	0.9	0.8	5.1	0.076	7.53	8.44	3.6	4.54	56.1±4.1	55.7	53.5		
GM1-C	Galeana	Mimbres	8	20-540	0.8	0.7	5.6	0.010	4.67	6.71	2.9	3.04	55±5.4	53.2	51.1		
GM1-D	Galeana	Mimbres	9	300-520	0.6	0.8	5.6	0.069	8.49	0.73	2.69	2.44	58.9±6.7	55.9	53.7		
Sherd-mean													**56.4±1.7**	**54.9±1.2**	**52.7±1.2**	**45.9±1.0**	**10.3**
PM2-A	Paquimé	Mimbres	11	150-570	1.0	0.9	7.0	0.086	7.12	8.41	1.43	3.17	56.7±7.0	57.9	55.6		
PM2-B	Paquimé	Mimbres	6	150-520	0.6	0.8	7.1	0.075	7.56	9.27	4.31	2.45	57.6±3.6	55.4	53.2		
PM2-C	Paquimé	Mimbres	6	20-495	0.8	0.8	31.0	0.059	5.97	7.56	2.43	2.82	51.6±1.0	53.2	51.1		
PM2-D	Paquimé	Mimbres	10	20-570	1.0	0.9	16.0	0.053	6.98	9.45	0.91	2.66	56.5±3.0	55.4	53.2		
Sherd-mean													**55.6±2.7**	**55.5±1.9**	**53.3±1.8**	**46.2±1.6**	**10.4**
VAM4-A	Villa Ahumada	Mimbres	8	20-450	0.4	0.7	3.3	0.089	3.28	4.96	5.14	3.01	63.4±5.5	61.5	59.0		
VAM4-B	Villa Ahumada	Mimbres	8	20-450	0.4	0.7	3.3	0.075	1.45	5.09	5.95	2.41	61.7±3.4	61.1	58.7		
VAM4-C	Villa Ahumada	Mimbres	7	20-450	0.4	0.8	5.5	0.085	2.17	4.68	6.6	1.98	60±4.1	59.7	57.3		
VAM4-D	Villa Ahumada	Mimbres	7	330-450	0.8	0.6	5.2	0.044	9.4	7.38	0.86	1.26	66.9±6.2	63.4	60.9		
Sherd-mean													**63.0±2.9**	**61.4±1.5**	**59.0±1.5**	**51.0±1.3**	**11.4**
GR1-B	Galena	Ramos	8	20-450	0.3	0.8	5.5	0.043	1.55	5.16	0.27	1.72	44.7±2.0	45.2	43.4		
Sherd-mean													***na***	***na***	***na***	***na***	***na***
PR1-A	Paquimé	Ramos	5	20-270	0.4	0.6	5.2	0.055	7.43	9.34	5.85	4.61	37.3±3.6	36.2	34.8		
PR1-B	Paquimé	Ramos	10	20-430	0.7	0.7	4.8	0.075	8.12	7.62	6.49	7.06	41.2±4.4	40.4	38.8		
PR1-C	Paquimé	Ramos	5	20-270	0.4	0.6	3.9	0.083	3.27	1.38	11.7	5.07	49.3±4.6	48.1	46.2		
PR1-D	Paquimé	Ramos	9	290-570	0.6	0.8	8.5	0.055	5.61	2.78	9.01	7.79	48.8±2.6	47.9	46.0		
Sherd-mean													**44.2±5.9**	**43.2±5.9**	**41.1±5.6**	**36.0±4.9**	**6.9**
PR4-A	Paquimé	Ramos	6	150-450	0.6	0.7	4.9	0.051	5.88	8.39	4.38	2.85	57.4±1.4	53.1	51.0		
PR4-C	Paquimé	Ramos	7	150-450	0.7	0.6	20.8	0.045	1.18	2.23	3.94	1.95	49.8±1.1	47.0	45.1		
PR4-D	Paquimé	Ramos	5	150-450	0.5	0.7	6.2	0.063	2.48	4.67	5.23	2.06	54.5±2.7	53.5	51.4		
PR4-E	Paquimé	Ramos	7	20-450	0.7	0.6	20.8	0.022	1.18	2.23	3.94	1.95	51.6±1.1	49.8	47.8		
Sherd-mean													**53.3±3.3**	**50.9±3.1**	**48.8±2.9**	**42.4±2.5**	**9.5**

VAR5-A	Villa Ahumada	Ramos	7	330-520	0.6	0.6	4.8	0.054	4.81	7.34	6.17	4.69	45.7±3.3	43.9	42.1	
VAR5-B	Villa Ahumada	Ramos	8	330-520	0.6	0.6	5.4	0.069	5.17	6.18	14.4	6.05	46.3±2.9	42.1	40.4	
VAR5-C	Villa Ahumada	Ramos	9	330-520	1.0	0.8	16.4	0.091	6.89	9.79	2.5	5.04	49.8±2.2	48.4	46.5	
VAR5-D	Villa Ahumada	Ramos	7	300-520	0.8	0.7	12.5	0.047	5.17	6.19	14.4	6.07	42.9±3.1	42.1	40.4	
Sherd-mean													**46.2±2.8**	**44.1±3.0**	**42.4±2.9**	**36.6±2.5**	**8.2**
VAR6-A	Villa Ahumada	Ramos	7	300-540	0.7	0.7	8.2	0.059	6.13	8.45	6.29	2.33	44.3±2.8	43.4	41.7	
VAR6-B	Villa Ahumada	Ramos	6	300-540	0.6	0.7	6.3	0.067	4.54	7.13	2.05	3.6	44.1±2.9	42.8	41.1	
VAR6-C	Villa Ahumada	Ramos	9	20-540	1.0	0.8	16.4	0.046	5.02	6.97	3.1	3.4	49.8±2.2	48.4	46.5	
Sherd-mean													**46.1±3.2**	**44.9±3.1**	**43.1±3.0**	**37.3±2.5**	**8.4**

Table 4

Sherd	Type	Age range (years AD)	
		Mahgoub local curve	**SHAWQ2k global model**
CH3-3	Mimbres	960-1020	500-820
CH3-A-2	Mimbres	980-1090	500-900
GM1	Mimbres	1000-1090	500-910
PM2	Mimbres	990-1100	500-920
VAM4	Mimbres	1040-1100	840-1600
	Mimbres	**960-1100**	**500-1600**
PR1	Ramos	1340-1600	500-880
PR4	Ramos	1300-1410	500-890
VAR5	Ramos	1360-1600	500-820
VAR6	Ramos	1340-1600	500-810
	Ramos	**1300-1600**	**500-890**